

# Mineralogy and Mineral Chemistry of the REE-Rich Black Sands in Beaches of the Kavala District, Northern Greece

Eftychia Peristeridou <sup>1</sup>, Vasilios Melfos <sup>1,\*</sup>, Lambrini Papadopoulou <sup>1</sup>, Nikolaos Kantiranis <sup>1</sup> and Panagiotis Voudouris <sup>2</sup>

<sup>1</sup> Faculty of Geology, Aristotle University of Thessaloniki, 54124 Thessaloniki, Greece; peristee@geo.auth.gr (E.P.); lambrini@geo.auth.gr (L.P.); kantira@geo.auth.gr (N.K.)

<sup>2</sup> Faculty of Geology & Geoenvironment, National and Kapodistrian University of Athens, 15784 Athens, Greece; voudouris@geol.uoa.gr

\* Correspondence: melfosv@geo.auth.gr

**Abstract:** The coastal area of the Kavala district, Northern Greece, is characterized by minerals enriched in rare earth elements (REE). The present study focuses on the mineralogy of the black sands from six different locations and the comprehensive mineral chemistry of the REE-bearing minerals, allanite-(Ce), epidote, monazite, thorite, zircon and titanite. Allanite-(Ce) is the most important carrier of light REE (LREE) in the studied black sands, reaching up to 23.24 wt %  $\Sigma$ REE. The crystal chemistry of allanite-(Ce) transitions into ferriallanite-(Ce), due to the significant involvement of Fe<sup>3+</sup>. High resolution backscattered electron (BSE) images were used to identify zoning that corresponds to variations in REE, Th and U. These modifications follow the exchange scheme: (Ca + (Fe<sup>3+</sup>, Al))<sub>-1</sub>(LREE, Y, Th, U + (Fe<sup>2+</sup>, Mg, Mn))<sub>+1</sub>. Epidotes may also contain up to 0.5 REE<sup>3+</sup> apfu. Monazite and thorite are found as inclusions in allanite-(Ce) and are enriched in Ce, La and Nd, together with Th and U. Some zircons are enriched in Hf, while some titanites host Nb and V.

**Citation:** Peristeridou, E.; Melfos, V.; Papadopoulou, L.; Kantiranis, N.; Voudouris, P. Mineralogy and Mineral Chemistry of the REE-Rich Black Sands in Beaches of the Kavala District, Northern Greece. *Geosciences* **2022**, *12*, 277. <https://doi.org/10.3390/geosciences12070277>

Academic Editor: Jesus Martinez-Frias, Pedro J.M. Costa

Received: 14 May 2022  
Accepted: 8 July 2022  
Published: 10 July 2022

**Publisher's Note:** MDPI stays neutral with regard to jurisdictional claims in published maps and institutional affiliations.



**Copyright:** © 2022 by the authors. Licensee MDPI, Basel, Switzerland. This article is an open access article distributed under the terms and conditions of the Creative Commons Attribution (CC BY) license (<https://creativecommons.org/licenses/by/4.0/>).

**Keywords:** rare earth elements (REE); black sands; Kavala; allanite subgroup, allanite-(Ce); epidote group; heavy minerals

## 1. Introduction

Critical metals are essential for future sustainable technologies, as the continuous growth in population and our dependence on technological innovation cause a rapid increase in their consumption. For this reason, the European Union (EU) Raw Materials Initiative assesses and releases periodically, since 2011, a list of metals, which are critical for the industry of new technology products and the “green” energy [1]. The 2020 EU Critical Raw Materials list was defined by two main parameters, the economic importance and the supply disruption of each commodity. The list of critical metals includes among others, the rare earth elements (REE) [2].

The REE are a group of 17 chemically similar elements including the lanthanides, from lanthanum to lutetium with atomic numbers 57 to 71, along with Y and Sc, with atomic number 39 and 21, as defined by the International Union of Pure and Applied Chemistry (IUPAC). The criticality of these metals is related to their application in the high-technology products and the clean “green” energy technologies, as there are concerns about supply constraints due to geological scarcity, a small number of producing countries and supply inelasticity driven by various byproduct features [1].

The REE are not necessarily rare in nature and are found in almost all rock formations. As they are suggested to be relatively immobile in various geological environments, they are widely used in petrogenetic studies. The least abundant REE are Tm and Lu, which are estimated to be 200 times more common than gold in the Earth's crust [3].

Thus, the REE are not rare in terms of average crustal abundance, but concentrated and economic deposits of REE are limited in number [4].

The global supply chain of rare earths is dominated by China, which controls >90% of the total production [5–7]. For over 50 years, carbonatites have been the primary source of Nb and REE, particularly the light rare earths (LREE) La, Ce, Pr and Nd, globally [7]. Since 2014, the largest carbonatite-type deposit, Bayan Obo (REE-Nb-Fe), in China, has been the primary supplier of the world's LREE [8,9]. There are over 100 potential REE ore minerals, but less than ten of them have been successfully processed for REE extraction [10,11]. One of the major issues in the REE metallurgy is the environmental impact due to the radioactivity that is related to elevated concentrations of uranium (U) and thorium (Th) in these deposits.

The natural deposits of rare earths can be classified into two categories based on their geological associations: primary and the secondary deposits. The primary, high-temperature deposits are associated with magmatic intrusions, especially carbonatites and alkaline–peralkaline igneous rocks, and with hydrothermal systems. The secondary, low-temperature deposits result from sedimentary or weathering processes, and are associated with placers, offshore sediments, bauxites, Ni-laterites, and ion-adsorption clays [5,6].

Placer deposits are considered as important REE resources and mainly occur in Malaysia, India, Australia, Brazil and Sri Lanka [5]. They form from the erosion, transportation and deposition of heavy minerals, in streambeds or at sand beaches. The streams and the wave energy are sufficient to carry away the low-density material, but not the heavy minerals, and a natural separation by gravity segregation may form the black sands. The term “black sands” is used for the dark-colored formations, which are enriched in heavy minerals, including ilmenite (Ti), rutile (Ti), zircon (Zr), monazite (REE) and xenotime (REE), and are a potential source for critical metals, offering the advantages of easy mechanical separation [10,11].

The black sands along the coast of Northern Aegean in Greece, and particularly between the Strymonikos Gulf and the Eleftheres Bay, of the Kavala district (Figure 1), have attracted the attention of many exploration research projects so far. The potential of these sands was initially described by Papadakis [12]. In 1981–1984, the Institute of Geology and Mineral Exploration (IGME) carried out extensive geological, mineralogical and geochemical research on the marine sediments of the Strymonikos plateau and the gulfs of Ierissos, Strymonikos and Kavala [13]. The strong anomalies of La and Zr in the sediments led IGME to conduct detailed research in this area, for the exploration of the polymetallic placers, during the period 1996–2000 [14,15]. The area was also investigated in the frame of the EuRare project (2013–2015) that focused on mapping and characterization of REE deposits in Europe [16]. Recently, natural radioactivity measurements and detailed geochemical analyses of enriched sand fractions were conducted in order to determine the source and the chemical character of the REE-rich minerals [16–21].

Beach placers of Kavala district are considered to be one of the most promising REE sources in Greece, since they demonstrate the most significant enrichment in  $\Sigma\text{REE} + \text{Y}$  [19,20] compared to the other REE occurrences in Greece. The purpose of the present work is to determine the nature of the REE-bearing minerals in the black sands from six locations between the Strymonikos Gulf and Eleftheres Bay, of the Kavala district in Northern Greece (Figure 1). The chemical composition of the REE-bearing minerals (allanite-(Ce), REE-rich epidote, epidote, monazite-(Ce), monazite-(La) and thorite) together with zircon and titanite is discussed for their enrichment in Ce, La, Nd, Nb, Hf, Th and U. The findings of this study show that the detailed characterization of the chemical composition of the REE-bearing minerals is important in understanding the correlation of rare earths with other structural elements of these minerals. In addition, scanning electron microscopy–backscattered electron (SEM–BSE) imaging reveals a fundamental study for the zoning patterns.

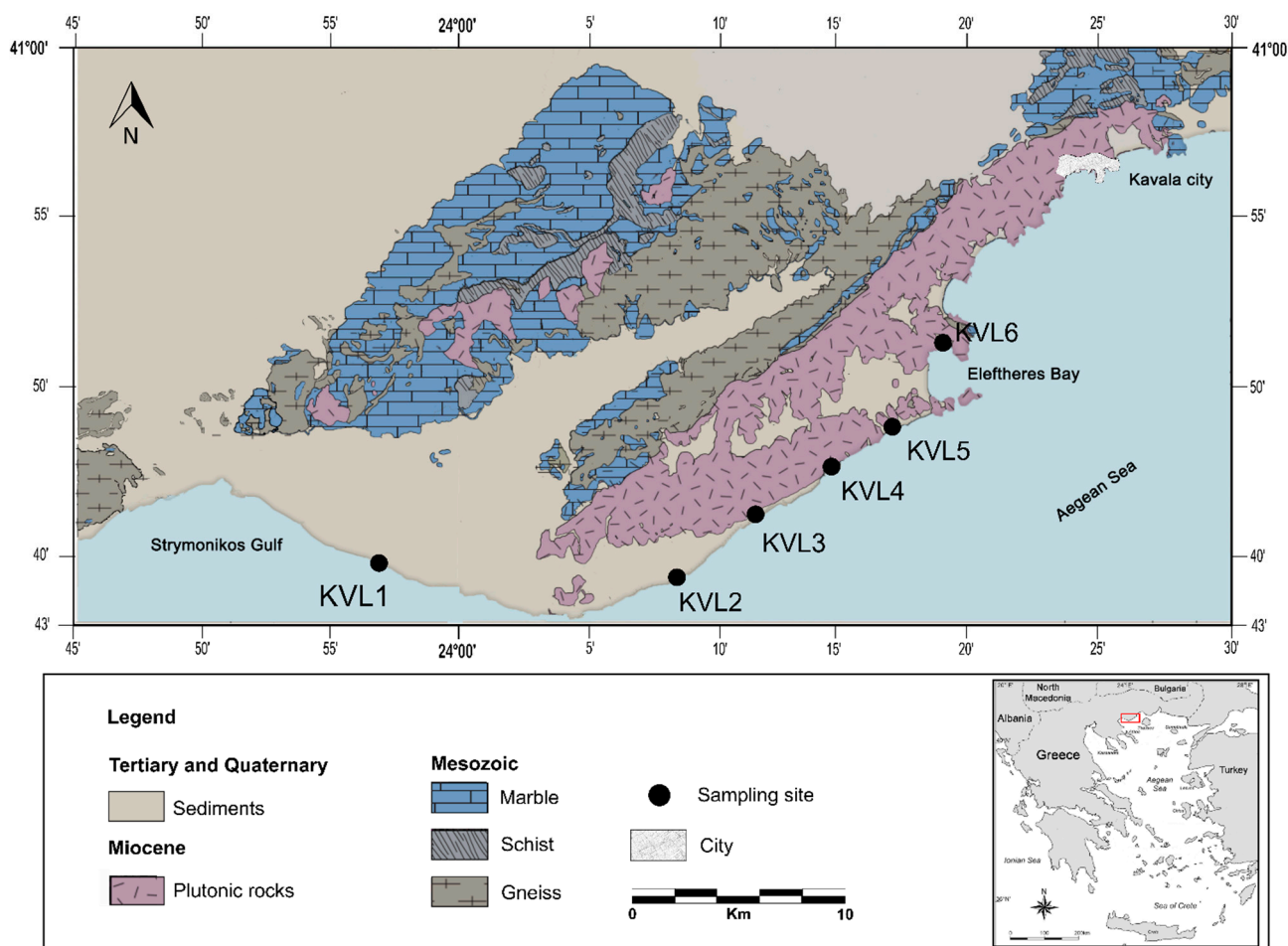


**Figure 1.** Simplified geological map of the area between the Strymonikos Gulf and Eleftheres Bay, of the Kavala district, with the sampling sites (KVL1–KVL6). Modified after [22–24].

## 2. Geological Setting

The study area is part of the Southern Rhodope Core Complex (SRCC) that comprises Paleozoic–Mesozoic orthogneisses overlain by massive Triassic marble horizons with schist and amphibolite intercalations [25–27]. These rocks were intruded by Upper Eocene to Middle Miocene plutonic rocks and covered by Oligocene to Miocene volcanics.

The dominant magmatic rock in the studied area is the Kavala (or Symvolon) pluton (Figure 1) that intruded the metamorphic basement along a detachment fault of SW–NE direction [28]. This pluton is a metaluminous, I-type intrusion with a calc-alkaline affinity [29]. The dominant rock type is an amphibole–biotite granodiorite, with numerous enclaves of tonalite, diorite, monzogranite and monzodiorite. All the rock types consist of similar mineralogical phases in different ratios. The main minerals are hornblende, biotite, muscovite, plagioclase, K-feldspar and quartz, while the accessory minerals include apatite, titanite, epidote, allanite, zircon, monazite, magnetite, thorite and ilmenite [29]. Occasionally discrete aplitic, pegmatitic and more mafic, usually porphyritic, veins and dikes, along with tourmaline-rich veins and breccias also occur [30,31].

Dating of titanite with U–Pb geochronology and hornblende with  $^{40}\text{Ar}/^{39}\text{Ar}$  spectra yielded the emplacement age for the Kavala pluton at 21 Ma [27]. The K–Ar biotite ages of  $15.5 \pm 0.5$  Ma [32] and  $17.8 \pm 0.8$  Ma [33] along with the 14–16 Ma Rb–Sr biotite age [34] were initially attributed to reset metamorphic ages, but Dinter and Royden [32] suggested that they are cooling ages of the footwall of the detachment fault system. This assumption is confirmed by the  $11.1 \pm 0.2$  –  $15.5 \pm 0.3$  Ma  $^{40}\text{Ar}/^{39}\text{Ar}$  dating results for biotite and K–feldspar from the central parts of the pluton [27].

Tertiary and mainly Quaternary nonconsolidated sedimentary deposits are also present (Figure 1). These deposits were formed from the action of the rivers that drain the metamorphic and igneous rocks, and consist of alluvial sediments, i.e., pebbles, gravels, sands, and clays. Along the coast, marine deposits of Holocene age, mainly sands, also occur [22–24].

### 3. Materials and Methods

A total of six black sand samples (Table 1) were collected along the coastal area of the Kavala district. The study area extends from the Strymonikos Gulf to Eleftheres Bay (Figure 1), over a 40 km long distance. Most of the sampling sites are adjacent to the Kavala intrusion and are characterized by thick horizons of black sands (up to 8 cm). The samples of the heavy mineral accumulations were collected from the surface or from these horizons (Figure 2). The preparation of the samples and the separation of the REE-rich minerals were performed at the laboratory of the Faculty of Geology at the Aristotle University of Thessaloniki.

**Table 1.** Code names and locations of the samples along the coast of the Kavala prefecture, shown in Figure 1.

Sample	Location
KVL1	Kariani
KVL2	Pirgos
KVL3	Mirtofito
KVL4	Eleochori
KVL5	Agia Marina
KVL6	Nea Peramos

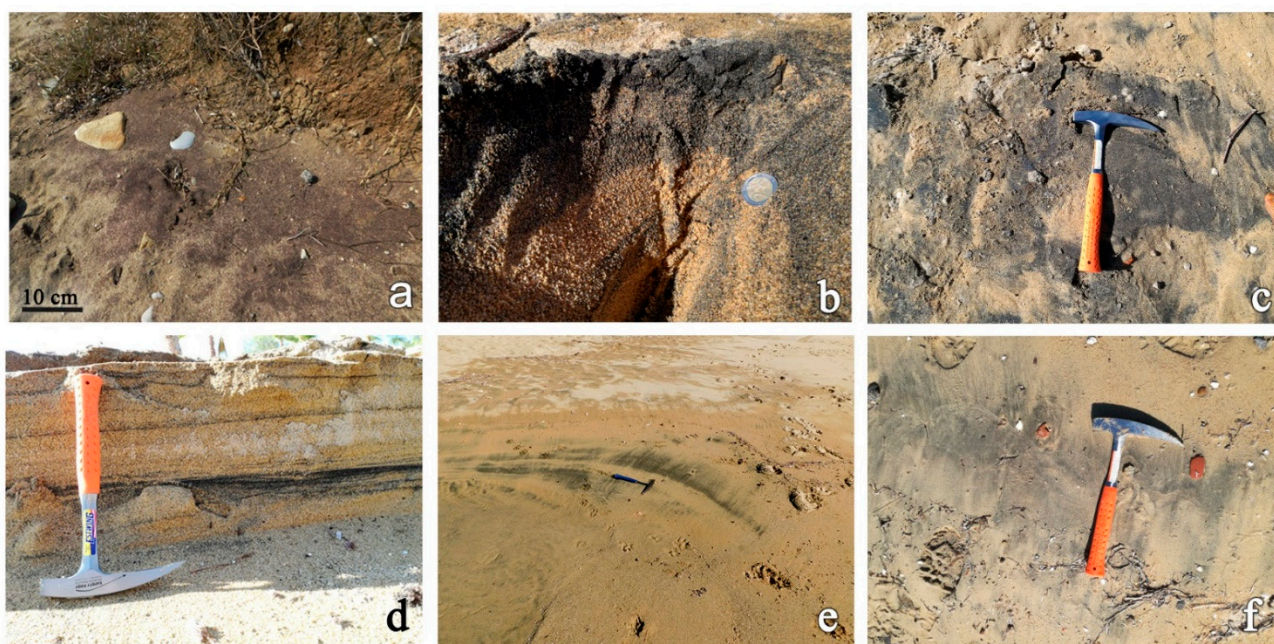


**Figure 2.** Sampling sites of the coast black sands at Kavala district. Heavy mineral accumulations were collected from the surface (a,c,e,f) and from horizons in the sand (b,d). The samples KVL1 to KVL6 are depicted in the images (a–f), respectively.

Initially, the samples were rinsed with water and then dried. The coarse fragments (organic material and rock gravels) were removed by sieving. Then, a preconcentration process was achieved with magnetic separation. For this reason, magnetite was removed

manually using a common magnet. Subsequently, a Frantz L-1 Isodynamic Magnetic Separator was used, under the settings of 0.8 A current, and inclined forward 15° and 25° sideways, for the enrichment of the REE-rich minerals. Two fractions, magnetic and non-magnetic, were obtained. The weight percentage of each fraction is shown in Table 2. Sample KVL1 contains the highest (59.89 wt %) and sample KVL6 the lowest magnetic fraction (22.60 wt %). This procedure led to the concentration of the heavy minerals in the magnetic fraction, due to their high magnetic susceptibility. The REE-bearing minerals, i.e., allanite-(Ce), epidote, monazite-(Ce), monazite-(La) and thorite, were separated under a binocular stereoscope (Leica Wild M10), and polished epoxy mounts of these minerals were prepared for detailed mineralogical observations.

**Table 2.** Magnetic fraction (MF) and nonmagnetic fraction (NMF) wt % for each of the studied samples.

Sample	MF %	NMF %
KVL1	59.89	40.11
KVL2	29.10	70.90
KVL3	26.64	73.36
KVL4	34.76	65.24
KVL5	27.32	72.68
KVL6	22.60	77.40

The mineralogical composition of the six magnetic fractions was determined by X-ray diffractometry (XRD), using a Philips PW1820/00 diffractometer, equipped with a PW 1710/00 controller and CuK $\alpha$  radiation (1.54056 Å wavelength) using a Ni-filter. The settings and the measurement parameters were settled with scanning speed of 0.5 sec, in a continuous scanning mode, and the scanning area of the goniometer was fixed between 3° and 63° at 35 kV and 25 mA. The Rietveld refinement of powder X-ray diffraction was performed with PROFEX software (version 4.3.5) [35] using the BGMN program.

The polished sections with the REE-bearing minerals were studied with a JEOL JSM-840A scanning electron microscope (SEM) (JEOL Ltd., Tokyo, Japan) equipped with an OXFORD INCA 300 energy dispersive system (EDS) (Oxford Instruments Ltd., Abingdon, UK) in the School of Sciences at Aristotle University of Thessaloniki. The operating conditions were a 20 kV accelerating voltage and 0.4 mA probe current, 80 s analysis time, and a beam diameter of ~1  $\mu$ m, in backscattering electron (BSE) mode. SEM–EDS microanalysis was targeted on the REE-bearing minerals and the following standards were used: SiK, AlK, KK, sanidine; NaK, albite; FeK, hematite; MgK, CaK, diopside; MnK, tephroite; TiK, rutile; ClK, sylvite; FK, fluorite; LaL, LaB<sub>6</sub>; CeL, CeO<sub>2</sub>; NdL, NdF<sub>3</sub>; EuL, EuF<sub>3</sub>; YL, Y; UM, synthetic UO<sub>3</sub>; ThM, synthetic ThO<sub>2</sub>; PK, GaP; ZrL, Zr; HfL, Hf; VK, vanadinite; NbL, synthetic Nb<sub>2</sub>O<sub>5</sub>.

## 4. Results

### 4.1. Mineralogical Composition of the REE-Bearing Minerals

The major and minor mineral phases of the magnetic fractions of the studied black sand samples were determined by XRD in combination with SEM–EDS analysis. The mineralogical composition consists mainly of silicates, Fe- and Ti-oxides, with minor phosphate minerals. The heavy mineral fraction, with specific gravity larger than that of quartz (~2.65), includes amphibole, epidote, hematite, goethite, mica, allanite, garnet, titanite, zircon, monazite, ilmenite, rutile, magnetite, chlorite and thorite (Table 3, Figure 3).

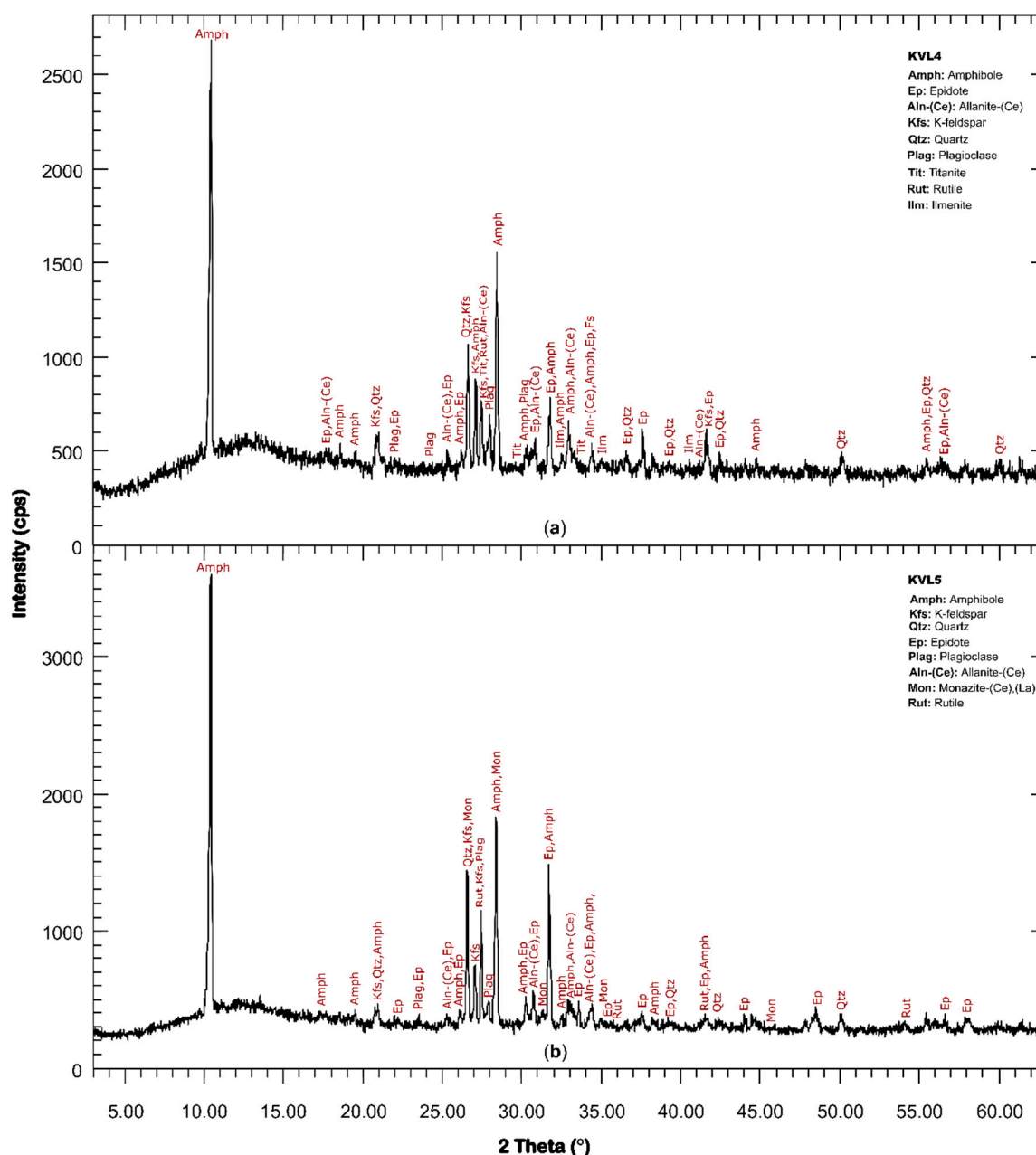


**Figure 3.** X-ray diffraction pattern of magnetic fraction of the black sand samples: (a) KVL4 and (b) KVL5.

The fraction of the heavy minerals was semiquantitatively determined, ranging from 62 to 100 wt %, while the remaining amount consists of quartz, K-feldspar and plagioclase (Table 3, Figure 3). Major components of five samples are amphibole and epidote, apart from KVL1, which is predominated by garnet (68 wt %). XRD results indicate that all samples of the magnetic fraction contain REE-bearing minerals (allanite-(Ce), epidote, monazite-(Ce), monazite-(La) and thorite). Allanite is present in all samples (2–5 wt %), while epidote appears to a greater extent, from 6 wt % in KVL1 to 38 wt % in KVL5. The minerals thorite and zircon were not detected in the fractions of all samples since they appear mainly as inclusions in allanite-(Ce) crystals. In addition, monazite-(Ce) and monazite-(La) constitute an alteration product of allanite and appear in fractures of the allanite-(Ce) grains.

**Table 3.** Mineralogical composition (%wt) of the magnetic fractions of the studied samples.

	KVL1	KVL2	KVL3	KVL4	KVL5	KVL6
Allanite-(Ce)	3	3	3	5	2	3
Amphibole	4	26	31	30	27	23
Chlorite	n.d.	n.d.	5	n.d.	n.d.	6
Epidote	6	20	32	21	38	28
Garnet	68	3	traces	traces	n.d.	traces
Goethite	n.d.	9	n.d.	n.d.	n.d.	n.d.
Hematite	4	1	14	traces	n.d.	1
Ilmenite	7	n.d.	n.d.	2	n.d.	n.d.
K-feldspar	n.d.	7	5	15	8	8
Magnetite	2	n.d.	traces	n.d.	traces	n.d.
Mica	6	5	n.d.	n.d.	n.d.	6
Monazite-(Ce), -(La)	traces	n.d.	n.d.	n.d.	2	2
Plagioclase	n.d.	16	n.d.	11	11	8
Quartz	n.d.	9	8	12	10	11
Rutile	n.d.	traces	1	2	2	n.d.
Thorite	traces	n.d.	n.d.	n.d.	traces	n.d.
Titanite	traces	traces	n.d.	2	traces	3
Zircon	traces	1	1	traces	traces	1
Total	100	100	100	100	100	100

n.d. = not detected.

#### 4.2. Chemical Composition of the REE-Bearing Minerals

The REE-bearing minerals in the black sands of the Kavala area are dominated by allanite-(Ce), REE-rich epidote, monazite-(Ce), monazite-(La) and thorite. Zircon and titanite have been reported in previous studies [16,19] as light REE (LREE) and heavy REE (HREE) carriers, respectively, based on the sensitive analytical method laser-ablation inductively coupled plasma mass spectrometry (LA-ICPMS), but the concentrations of the REE were under the detection limits of the analytical method (SEM-EDS) used in the present study. Zircon from the Kavala area, apart from Zr, contains minor amounts of Hf, U and Th, whereas V and Nb occur in traces in titanite. Thorium and U, which are commonly associated with REE-bearing minerals, are incorporated in the crystal structure of the most minerals of the magnetic fragment, except titanite.

##### 4.2.1. Composition of Allanite

Allanite constitutes the most REE-rich member of the epidote-group minerals, and its general chemical formula is  $\{A1^{2+}A2^{2+}M1^{3+}M2^{3+}M3^{2+}\}(Si_2O_7)(SiO_4)O(OH)$  [36]. The A1 site is dominated by Ca, while in the A2 site, the excess Ca and the cations Sr,  $Pb^{2+}$ ,  $Mn^{2+}$ ,  $REE^{3+}$ , Th and U are incorporated. The cations Al,  $Fe^{3+}$ ,  $Fe^{2+}$ ,  $Mn^{3+}$ ,  $Mn^{2+}$ , Mg,  $Cr^{3+}$  and  $V^{3+}$  are distributed in the three structurally different octahedral M sites, M1, M2 and M3 [37,38].

As compared with the epidote and the clinozoisite subgroups, allanite is characterized by a dominance of  $REE^{3+}$  against  $Ca^{2+}$  in the A2 site, with  $(REE)_2O_3$  concentration >3 wt %, and  $REE^{3+} > 0.5$  atoms per formula unit (apfu) [39]. Cerium is the most common REE in allanite, but there are available literature data for La- and Y-dominant species, presenting distinct allanite mineral species [39,40]. In the M3 site,  $Fe^{3+}$  of epidote or  $Al^{3+}$  of clinozoisite is replaced by  $Fe^{2+}$  of allanite [36,39–41].

The classification of the analyzed allanite and epidote from Kavala is shown in the three major end-members (epidote–allanite–clinozoisite) ternary plot (Figure 4). The analyses with REE + Y content between 0.5 and 0.1 apfu are referred to as REE-rich epidotes, while those with <0.1 apfu, as epidotes. Microanalyses from Kavala distinguish three

types of minerals: epidote, REE-rich epidote and allanite-(Ce), whereas clinozoisite is absent.

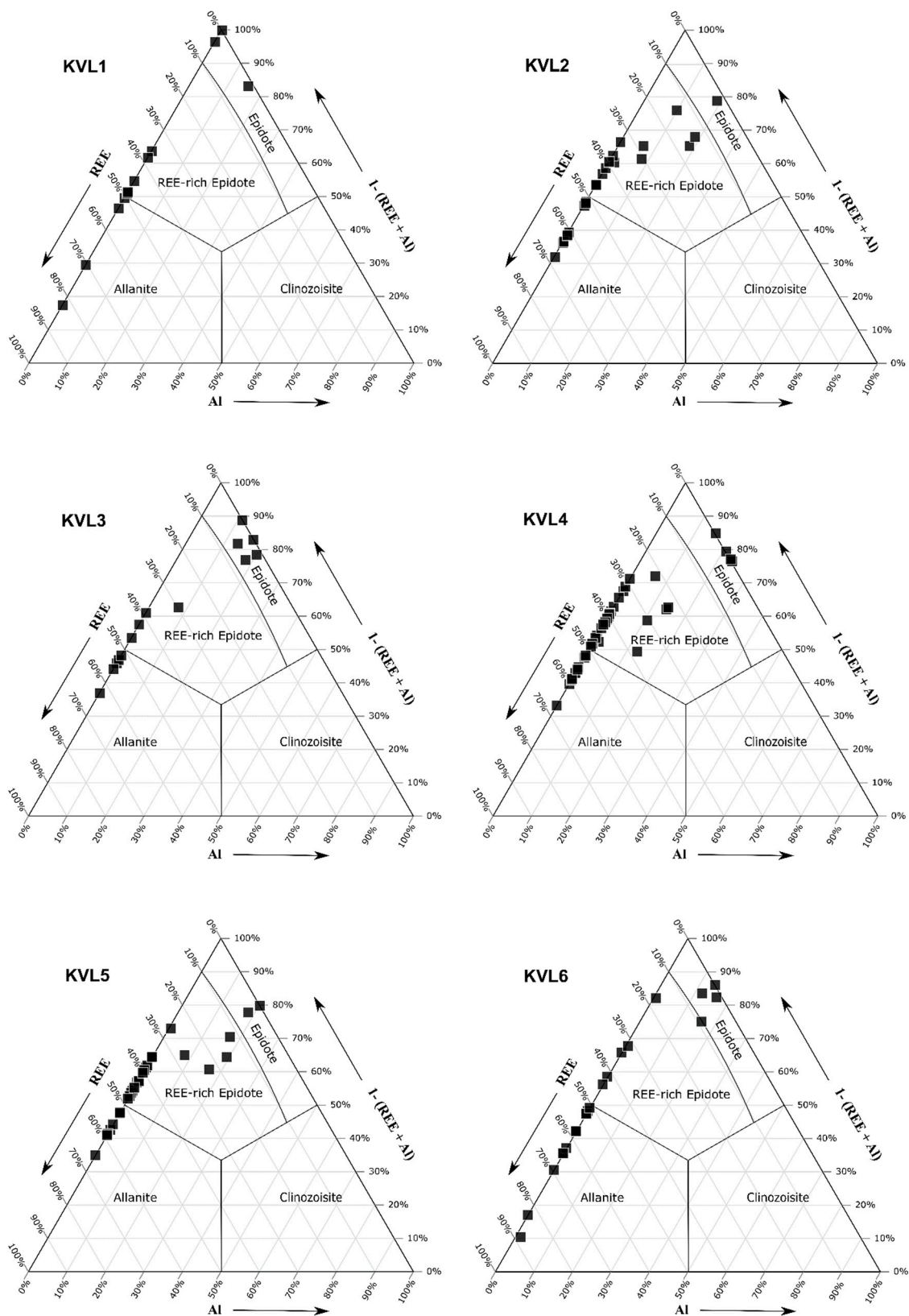
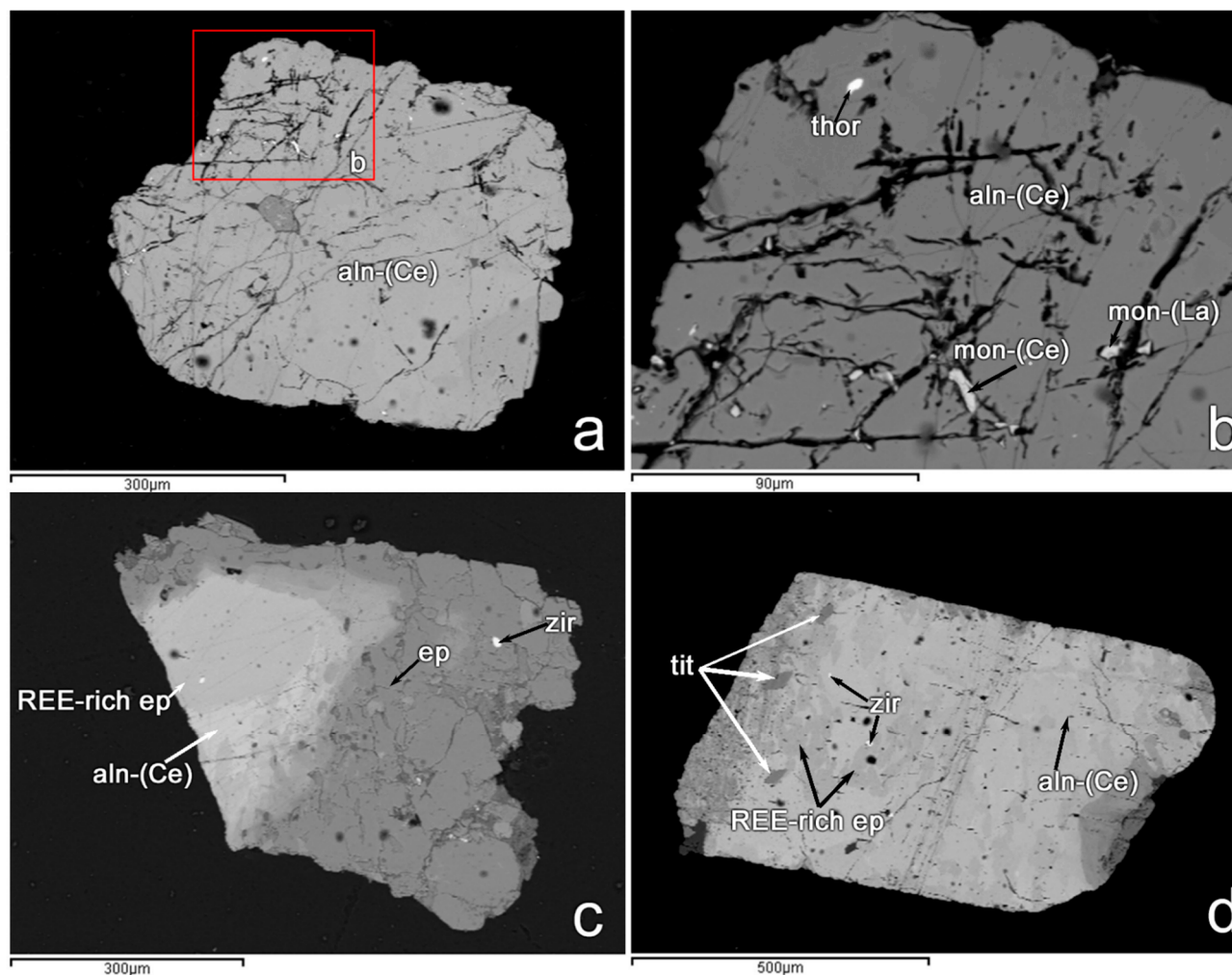


Figure 4. Epidote–Allanite–Clinozoisite ternary plots [ 42] for the six studied samples.

Allanite-(Ce) is the major REE-bearing mineral phase in the studied black sands from Kavala. It occurs as euhedral to subhedral crystals with dark brown to black color. Its morphology shows a tabular habit, while it also occurs as prismatic to acicular grains with no apparent cleavage. Allanite-(Ce) grains range in size from 0.2 to 0.8 mm, and sometimes they are found as inclusions in quartz or epidote. The SEM–BSE images demonstrate a homogenous appearance (Figure 5a), although in some cases allanite-(Ce) shows variations in brightness within a single crystal, indicating variances to the REE content (Figure 5c-d). Additionally, it rarely contains inclusions of zircon (Figure 5c-d), thorite (Figure 5b), titanite (Figure 5d) and monazite-(Ce) (Figure 5b).



**Figure 5.** SEM–BSE images of allanite grains from Kavala. (a,b) Homogeneously colored allanite-(Ce) with inclusions of thorite and monazite-(Ce). (c) Heterogeneous grain showing the enrichment of REE in the brighter parts. The straight limits indicate the progressive hydrothermal alteration of allanite-(Ce) to REE-rich epidote and finally to epidote. Inclusions of zircon are also present. (d) Heterogeneous, hydrothermally altered allanite-(Ce) with inclusions of titanite and zircon. aln-(Ce) = allanite-(Ce), thor = thorite, mon-(Ce) = monazite-(Ce), mon-(La) = monazite-(La), REE-rich ep = epidote (with more than 0.1  $\Sigma$ REE apfu), ep = epidote, tit = titanite.

Multiple grains of allanite and several points within a single grain were analyzed for 26 elements (Table 4). Apart from Ca, Al, Si, Fe and LREE (Ce, La), the concentration of the other elements, such as Mg, Mn, U, Th, Nd, Eu and Y, are below the detection limit or rarely exceed 0.3 atoms per formula unit. According to the structure refinement described by Armbruster et al. [39], the structural formula of allanite was calculated on the basis of 12.5 oxygens and 8 cations per formula unit ( $\Sigma_{A+M+T} = 8$ ).

**Table 4.** Representative microanalyses (wt %) and calculated formulae of allanite-(Ce) from the black sands at Kavala.

	KVL1 1.3	KVL2 5.2	KVL2 5.4	KVL3 1.2	KVL3 1.3	KVL4 3.1	KVL6 2.3	KVL6 3.1	KVL6 3.3	KVL6 3.4
SiO <sub>2</sub>	30.43	31.63	32.11	31.73	32.74	31.87	30.01	32.21	31.40	32.48
Al <sub>2</sub> O <sub>3</sub>	13.04	15.19	16.75	16.14	17.28	14.72	15.14	16.75	15.88	16.78
FeO*	15.57	14.22	13.71	13.61	14.08	13.52	14.02	14.09	13.82	11.97
MgO	1.88	1.29	1.31	0.99	0.81	1.86	1.27	1.13	1.03	1.17
MnO	bdl	0.68	bdl	0.45	0.51	0.92	bdl	bdl	1.19	1.03
CaO	10.82	12.56	14.32	13.72	15.22	12.82	10.85	14.47	13.27	14.44
La <sub>2</sub> O <sub>3</sub>	4.43	6.16	3.84	5.71	5.56	6.50	7.12	5.05	6.99	5.15
Ce <sub>2</sub> O <sub>3</sub>	12.72	10.23	8.65	8.85	8.86	11.44	13.59	8.07	9.73	7.15
Nd <sub>2</sub> O <sub>3</sub>	3.91	1.83	2.66	1.14	1.50	1.63	2.52	1.29	1.67	1.72
Eu <sub>2</sub> O <sub>3</sub>	2.35	bdl	0.34	bdl	0.13	bdl	bdl	1.42	bdl	bdl
Y <sub>2</sub> O <sub>3</sub>	bdl	1.10	bdl	0.75						
UO <sub>3</sub>	bdl	bdl	bdl	bdl	bdl	1.00	bdl	bdl	bdl	bdl
ThO <sub>2</sub>	2.00	2.57	3.19	3.81	bdl	1.00	1.70	2.30	1.89	3.02
Total	97.15	97.46	96.89	96.14	96.69	97.29	96.22	96.77	96.87	95.67
Chemical Formulae Calculated on the Basis of 12.5 O										
Si	2.963	2.969	2.953	2.976	2.952	2.984	2.928	2.955	2.934	2.991
Al	0.037	0.031	0.047	0.024	0.048	0.016	0.072	0.045	0.066	0.009
<i>T</i>	3.000	3.000	3.000	3.000	3.000	3.000	3.000	3.000	3.000	3.000
Fe <sup>3</sup>	0.541	0.350	0.235	0.242	0.209	0.391	0.328	0.235	0.319	0.189
Al	0.459	0.650	0.768	0.760	0.789	0.609	0.669	0.766	0.683	0.813
<i>M1</i>	1.000	1.000	1.003	1.002	0.998	1.000	0.997	1.001	1.002	1.002
Al	1.000	1.000	1.000	1.000	1.000	1.000	1.000	1.000	1.000	1.000
<i>M2</i>	1.000	1.000	1.000	1.000	1.000	1.000	1.000	1.000	1.000	1.000
Mn <sup>2</sup>	0.000	0.054	0.000	0.036	0.039	0.073	0.000	0.000	0.094	0.081
Fe <sup>2</sup>	0.615	0.531	0.436	0.514	0.339	0.339	0.645	0.426	0.410	0.388
Mg	0.273	0.180	0.180	0.138	0.108	0.259	0.184	0.154	0.144	0.160
Fe <sup>3</sup>	0.112	0.235	0.384	0.312	0.514	0.329	0.171	0.420	0.352	0.371
<i>M3</i>	1.000	1.000	1.000	1.000	1.000	1.000	1.000	1.000	1.000	1.000
<i>M</i>	3.000	3.000	3.003	3.002	2.998	3.000	2.997	3.001	3.002	3.002
Ca	1.000	1.000	1.000	1.000	1.000	1.000	1.000	1.000	1.000	1.000
<i>A1</i>	1.000	1.000	1.000	1.000	1.000	1.000	1.000	1.000	1.000	1.000
Ca	0.128	0.263	0.411	0.379	0.471	0.287	0.134	0.422	0.329	0.425
REE	0.826	0.625	0.519	0.540	0.530	0.670	0.830	0.528	0.630	0.473
Y	0.000	0.055	0.000	0.000	0.000	0.000	0.000	0.000	0.000	0.037
U	0.000	0.000	0.000	0.000	0.000	0.021	0.000	0.000	0.000	0.000
Th	0.044	0.055	0.067	0.081	0.000	0.021	0.038	0.048	0.040	0.063
<i>A2</i>	0.998	0.998	0.997	1.000	1.001	0.999	1.002	0.998	0.999	0.998
<i>A</i>	1.998	1.998	1.997	2.000	2.001	1.999	2.002	1.998	1.999	1.998
Σ <sub>cation</sub> charge	24.985	24.990	24.993	24.996	24.992	24.981	25.000	24.998	25.000	25.000
Fe <sub>ox</sub>	0.515	0.524	0.587	0.519	0.681	0.680	0.436	0.606	0.621	0.591

FeO\*: total iron as FeO; bdl: below detection limit.

The content of the rare earths in allanite-(Ce) from Kavala varies between 14.78 and 23.24 wt % in total. Lanthanum (III) oxide (La<sub>2</sub>O<sub>3</sub>) ranges from 3.84 to 7.12 wt %, Ce<sub>2</sub>O<sub>3</sub> from 7.15 to 14.75 wt %, Nd<sub>2</sub>O<sub>3</sub> up to 3.91 wt %, Eu<sub>2</sub>O<sub>3</sub> up to 2.35 wt % and Y<sub>2</sub>O<sub>3</sub> up to 1.10 wt %. Allanite-(Ce) also contains up to 3.81 wt % ThO<sub>2</sub>. Similar concentrations have been presented previously [20,21].

The ratio  $\text{Fe}^{2+}/\text{Fe}^{3+}$  was calculated until the total cation charges were equal to 25. Manganese is assumed to be as  $\text{Mn}^{2+}$ ; this assumption does not introduce large stoichiometric errors because  $\text{Mn}^{2+}$  is a minor constituent [43]. Epidote is characterized by a strong preference for  $\text{Fe}^{3+}$  in the M3 site, whereas the cation  $\text{Fe}^{2+}$  occupies the octahedral M3 site in allanite. Ferriallanite, almost identical to allanite, is constituted by essential  $\text{Fe}^{2+}$  quantity and exhibits  $\text{Fe}^{3+}$  dominance in the octahedral M1 site [44]. The average chemical formula of the allanite from Kavala is:

$(\text{REE}_{0.597}\text{Ca}_{1.360}\text{Th}_{0.047}\text{U}_{0.002}) (\text{Al}_{1.732}\text{Fe}^{2+}_{0.443}\text{Fe}^{3+}_{0.620}\text{Mn}_{0.052}\text{Mg}_{0.154}) (\text{Si}_{2.962}\text{Al}_{0.038}\text{O}_{12}) (\text{OH})$ . In this formula,  $\text{REE}_{0.597}$  represents the sum of the atoms of individual lanthanides and yttrium contents, i.e.,  $\text{La}_{0.184}$ ,  $\text{Ce}_{0.331}$ ,  $\text{Nd}_{0.070}$ ,  $\text{Eu}_{0.007}$  and  $\text{Y}_{0.005}$ . The  $\Sigma\text{REE} + \text{Y}$  content in all analyzed allanites from Kavala varies between 0.505 and 0.830 apfu. Thorium content reaches 0.081 apfu, while U is typically present in lower concentrations, up to 0.021 apfu, when it is present.

The graphic illustration of  $\text{Al}_{\text{tot}}$  vs.  $\text{REE} + \text{Y}$  (apfu), proposed by [38,45], shows the chemical relationship between ferriallanite, allanite, epidote and clinozoisite (Figure 6). This diagram can be used to estimate the  $\text{Fe}_{\text{ox}} = \text{Fe}^{3+}/\text{Fe}_{\text{tot}}$  values from the lines radiating by the clinozoisite end member; however, these values are slightly different from the  $\text{Fe}_{\text{ox}}$  that were calculated from the microanalysis based on [38] (Tables 4 and 5). The REE-enriched allanites plot within the area between allanite and ferriallanite, indicating a sufficient ferriallanite component with significant  $\text{Fe}^{3+}$  incorporation in the composition of the allanite. The plotted  $\text{Al}_{\text{tot}}$  values of allanite range between 1.34 and 1.96 apfu. The plotted  $\text{Fe}_{\text{ox}}$  values are  $< 0.6$ .

#### 4.2.2. Composition of Epidote

The epidote mineral subgroup is described by the general chemical formula  $\{\text{A1}^{2+}\text{A2}^{2+}\text{M1}^{3+}\text{M2}^{3+}\text{M3}^{3+}\} (\text{Si}_2\text{O}_7)(\text{SiO}_4)\text{O}(\text{OH})$  [39,41,46], where the A1 and A2 sites are dominated by Ca, although Mn, REE (mainly Ce), Th and U are usually incorporated. The three distinct octahedral sites M1, M2 and M3 are generally occupied by Al, and are commonly substituted by  $\text{Fe}^{3+}$ . Epidote may also contain small amounts of Mn, Mg,  $\text{Fe}^{2+}$ , Sr, Cr and V. The subgroup of epidote is derived from the clinozoisite subgroup by homovalent substitution in the M sites of the type:  $\text{Al}^{3+} \leftrightarrow \text{Fe}^{3+}$  [39].  $\text{Fe}^{3+}$  strongly favors the M3 site. However, when total  $\text{Fe}^{3+}$  content is high, it substitutes in the M1 site. The term REE-rich epidote refers to epidotes with  $0.1 < \text{REE} < 0.5$  apfu in the A1 site.

Epidote in the black sands at Kavala is found as discrete anhedral grains or as clusters of grains around allanite-(Ce), and has a light green to yellow-green color, ranging in length from 400  $\mu\text{m}$  to 2 mm (Figure 7a). In the SEM–BSE images, the epidote grains show either homogeneous internal textures (Figure 7b) or they present zoning patterns of progressive hydrothermal alteration of allanite-(Ce) (Figure 7c). Epidote rims are significantly lower in REE content and thus darker in the SEM–BSE images (Figure 7c). In addition, the allanite-(Ce) crystals with varying brightness are linked to fluctuations in the REE contents, so that the darker areas are depleted in REE and are characterized as REE-rich epidote in contrast to the brighter core.

The analyzed epidotes display elevated REE contents reaching 15.75 wt %  $\Sigma\text{REE}$  in the REE-rich epidote (Table 5). Calcium dominates in the A site and decreases with increasing REE content. Thorium rarely exceeds 0.035 apfu in the REE-poor epidote and reaches 0.104 apfu in the REE-rich epidote. Uranium in epidote participates in smaller quantities, reaching up to 0.017 apfu. The SEM–EDS analyses yielded the following representative chemical formula for the REE-rich epidotes:

$(\text{Ca}_{1.595}\text{REE}_{0.369}\text{Th}_{0.035}\text{U}_{0.001}) (\text{Al}_{1.915}\text{Fe}^{3+}_{0.683}\text{Fe}^{2+}_{0.284}\text{Mg}_{0.080}\text{Mn}_{0.037}) (\text{Si}_{2.958}\text{Al}_{0.042}\text{O}_{12}) (\text{OH})$

and for the epidotes:

$(\text{Ca}_{1.976}\text{REE}_{0.020}\text{Th}_{0.004}\text{U}_{0.001}) (\text{Al}_{1.903}\text{Fe}^{3+}_{0.939}\text{Fe}^{2+}_{0.001}\text{Mg}_{0.006}\text{Mn}_{0.031}) (\text{Si}_{2.973}\text{Al}_{0.044}\text{O}_{12}) (\text{OH})$ .

**Table 5.** Representative microanalyses (wt %) and calculated formulae of REE-rich epidote and epidote from the black sands at Kavala.

	REE-Rich Epidote						Epidote		
	KVL1 3.3	KVL4 2.2	KVL4 2.5	KVL5 2.3	KVL5 7.1	KVL5 5.8	KVL6 5.1	KVL4 3.5	KVL5 14.3
SiO <sub>2</sub>	33.14	33.44	34.10	32.14	32.93	32.27	33.03	37.20	36.77
Al <sub>2</sub> O <sub>3</sub>	17.34	19.05	21.11	17.16	18.03	16.28	18.17	23.77	23.82
FeO *	13.15	13.19	12.37	13.40	12.81	13.63	13.27	11.48	12.94
MgO	0.93	bdl	bdl	1.08	0.63	1.13	0.59	bdl	bdl
MnO	0.66	bdl	0.53	0.64	2.42	0.93	0.55	0.34	0.98
CaO	15.83	15.56	18.67	14.47	16.67	14.78	15.84	23.32	23.51
La <sub>2</sub> O <sub>3</sub>	3.70	5.17	2.52	4.81	0.92	4.00	2.83	bdl	bdl
Ce <sub>2</sub> O <sub>3</sub>	7.31	7.05	3.96	9.70	3.25	6.85	6.89	bdl	bdl
Nd <sub>2</sub> O <sub>3</sub>	bdl	1.97	1.22	1.24	2.43	3.53	1.84	bdl	bdl
Eu <sub>2</sub> O <sub>3</sub>	bdl	bdl	bdl	bdl	bdl	bdl	1.24	bdl	bdl
Y <sub>2</sub> O <sub>3</sub>	bdl	bdl	bdl	bdl	3.11	bdl	bdl	bdl	bdl
UO <sub>3</sub>	bdl	bdl	0.87	0.76	bdl	bdl	bdl	bdl	bdl
ThO <sub>2</sub>	5.08	1.75	1.01	2.03	3.28	3.18	2.96	0.23	bdl
Total	97.15	97.19	96.36	97.42	96.48	96.58	97.20	96.33	98.02
Chemical Formulae Calculated on the Basis of 12.5 O									
Si	2.990	2.999	2.932	2.934	2.909	2.963	2.963	2.972	2.924
Al	0.010	0.001	0.068	0.066	0.091	0.037	0.037	0.028	0.076
T	3.000	3.000	3.000	3.000	3.000	3.000	3.000	3.000	3.000
Fe <sup>3</sup>	0.168	0.000	0.000	0.219	0.209	0.274	0.117	0.207	0.207
Al	0.834	1.003	1.001	0.780	0.787	0.725	0.884	0.793	0.793
M1	1.002	1.003	1.001	0.999	0.996	0.999	1.001	1.000	1.000
Al	1.000	1.000	1.000	1.000	1.000	1.000	1.000	1.000	1.000
M2	1.000	1.000	1.000	1.000	1.000	1.000	1.000	1.000	1.000
Mn <sup>2</sup>	0.051	0.000	0.039	0.049	0.181	0.072	0.042	0.023	0.066
Fe <sup>2</sup>	0.398	0.546	0.155	0.328	0.143	0.358	0.382	0.000	0.000
Mg	0.125	0.000	0.000	0.147	0.082	0.155	0.079	0.000	0.000
Fe <sup>3</sup>	0.426	0.444	0.735	0.476	0.594	0.415	0.497	0.560	0.568
Al	0.000	0.010	0.071	0.000	0.000	0.000	0.000	0.000	0.000
M3	1.000	1.000	1.000	1.000	1.000	1.000	1.000	1.001	0.998
M	3.002	3.003	3.001	2.999	2.996	2.999	3.001	3.001	2.998
Ca	1.000	1.000	1.000	1.000	1.000	1.000	1.000	1.000	1.000
A1	1.000	1.000	1.000	1.000	1.000	1.000	1.000	1.000	1.000
Ca	0.530	0.496	0.720	0.416	0.578	0.454	0.523	0.996	1.003
REE	0.364	0.466	0.243	0.527	0.212	0.482	0.417	0.000	0.000
Y	0.000	0.000	0.000	0.000	0.146	0.000	0.000	0.000	0.000
U	0.000	0.000	0.017	0.015	0.000	0.000	0.000	0.000	0.000
Th	0.104	0.036	0.020	0.042	0.066	0.066	0.006	0.004	0.000
A2	0.998	0.998	1.000	0.999	1.002	1.0002	1.000	1.000	1.003
A	1.998	1.998	2.000	1.999	2.002	2.002	2.000	2.000	2.003
Σcharge cation	24.990	24.996	24.990	24.981	24.985	24.993	25.000	24.960	24.858
Fe <sub>ox</sub>	0.599	0.448	0.826	0.679	0.849	0.658	0.616	1.000	1.000

FeO \*: total iron as FeO; bdl: below detection limit.

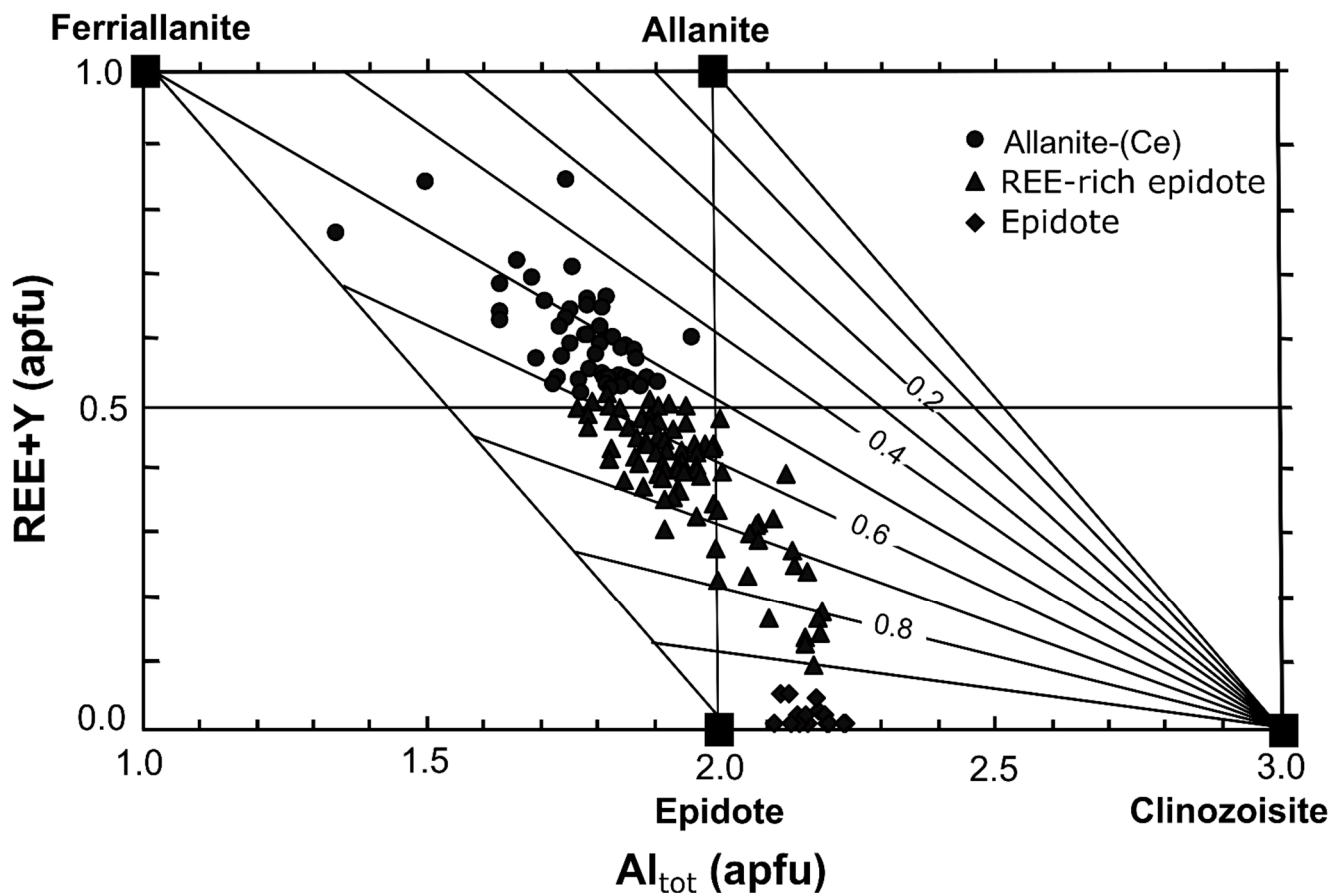


**Figure 6.**  $Al_{tot}$  vs. REE + Y (apfu) diagram after [45], showing the position of the studied epidote mineral group in the ferriallanite–allanite–epidote–clinzoisite system. Isolines represent the  $Fe_{ox} = Fe^{3+}/Fe_{tot}$  ratio.

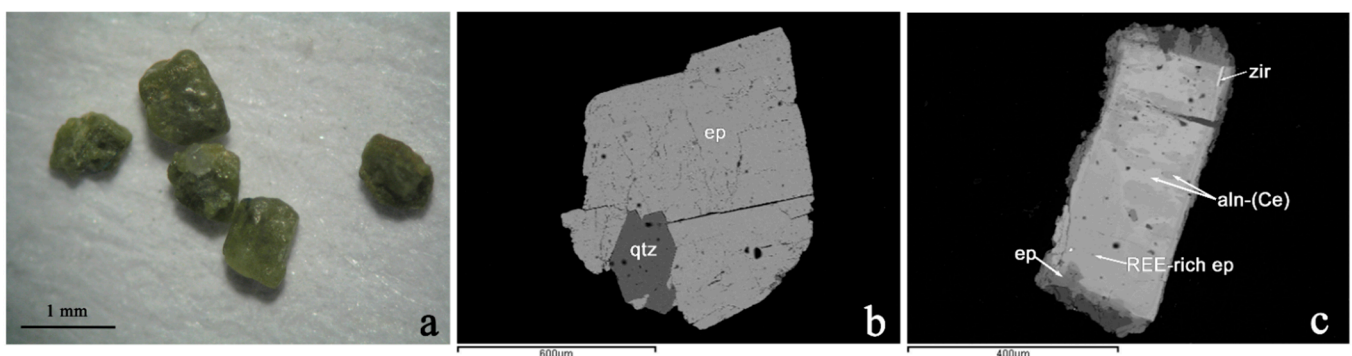


**Figure 7.** (a) Epidote grains under binocular microscope; (b) SEM–BSE image of epidote intergrown with quartz; (c) SEM–BSE image illustrating a grain with epidote in the rim and REE-rich epidote and allanite-(Ce) in the core. The ragged edges between REE-rich epidote and allanite-(Ce) zones are attributed to hydrothermal alteration of epidote. Zircon inclusions are also present. Ep = epidote, qtz = quartz, zir = zircon, aln-(Ce) = allanite-(Ce), REE-rich ep = epidote (with more than 0.1  $\Sigma$ REE apfu).

#### 4.2.3. Composition of Monazite and Thorite

Monazite in the studied samples is rare and usually forms tiny ( $\sim 40 \mu\text{m}$ ) columnar grains with a relic appearance and overgrown by allanite-(Ce). Occasionally, monazite occurs along the fractures of allanite-(Ce) (Figure 5b). Table 6 reports representative SEM–EDS analyses carried out in the monazite grains of the Kavala black sands.

Monazite chemical composition presents a strong variability in the contents of  $\Sigma\text{REE}_2\text{O}_3$  (22.2–55.21 wt %) and  $\text{ThO}_2$  (6.33–49.61 wt %). The KVL1-1.4 grain contains 21.69 wt % Ce, and is characterized as monazite-(Ce), including minor concentrations of La and Nd, while the KVL1-1.5 grain is dominated by La (20.64 wt %), and is characterized as monazite-(La). The higher content of Th in the KVL5-7.5 grain (49.61 wt % Th) is coupled with lower  $\Sigma\text{REE}$  (22.23 wt %) in comparison to Th-poor monazite-(La) (Table 6). The KVL5-7.5 grain may represent a monazite–cheralite solid-solution mineral phase.

Thorite is an accessory phase in the KVL1 sample, forming bleb-like inclusions (~10  $\mu\text{m}$  across) in allanite-(Ce). Apart from Th (almost 75.95 wt %), it contains La (1.34 wt %) and Ce (2.48 wt %) (Table 6).

**Table 6.** Representative microanalyses (wt %) and calculated formulae of monazite mineral group and thorite from the black sands at Kavala.

	KVL1.1 4	KVL1.1 5	KVL5.7 5	KVL1.4 1
	Monazite-(Ce)	Monazite-(La)	Monazite–Cheralite	Thorite
$\text{P}_2\text{O}_5$	31.25	32.26	25.94	bdl
$\text{SiO}_2$	bdl	bdl	bdl	19.87
CaO	6.07	5.82	1.81	0.29
$\text{La}_2\text{O}_3$	13.08	20.64	8.27	1.34
$\text{Ce}_2\text{O}_3$	21.69	19.49	7.98	2.48
$\text{Nd}_2\text{O}_3$	5.92	15.08	5.98	bdl
$\text{ThO}_2$	21.45	6.33	49.61	75.95
Total	99.45	99.62	99.58	99.94
Chemical Formulae Calculated on the Basis of 4 O				
P	1.011	1.015	0.959	0.000
Si	0.000	0.000	0.000	1.036
Ca	0.248	0.232	0.085	0.016
La	0.184	0.283	0.133	0.026
Ce	0.303	0.265	0.128	0.047
Nd	0.081	0.200	0.093	0.000
Th	0.186	0.054	0.493	0.901
Total	2.014	2.049	1.891	2.026

bdl = below detection limit.

#### 4.2.4. Composition of Zircon and Titanite

Numerous zircon inclusions are found in allanite-(Ce), epidote and titanite of the black sands at Kavala. Microanalyses (Table 7) demonstrated an enrichment of  $\text{HfO}_2$  (up to 1.73 wt %), and  $\text{UO}_2$  (up to 2.72 wt %) in some grains. Rare earths were not observed. Titanite is a rare mineral phase in the magnetic fraction of the black sands. Under the binocular microscope they are reddish brown to colorless with a mean grain size of 0.3 mm. It is found also as inclusions in allanite-(Ce) and magnetite. Representative microanalyses of titanite are shown in Table 8.  $\text{V}_2\text{O}_5$  ranges between 0.57 and 0.62 wt %, and  $\text{Nb}_2\text{O}_5$  from 0.55 to 1.03 wt %.  $\text{REE}_2\text{O}_3$ ,  $\text{ThO}_2$  and  $\text{UO}_3$  are below the detection limits.

**Table 7.** Representative microanalyses (wt %) and calculated formulae of zircon from the black sands at Kavala.

	KVL3 3.5	KVL3 6.7	KVL4 1.6	KVL4 6.6	KVL6 2.5
SiO <sub>2</sub>	32.34	31.85	32.26	32.07	32.09
ZrO <sub>2</sub>	67.12	65.33	65.66	64.63	64.06
ThO <sub>2</sub>	bdl	bdl	bdl	1.93	1.42
HfO <sub>2</sub>	bdl	bdl	1.73	bdl	1.19
UO <sub>3</sub>	bdl	2.24	bdl	1.09	1.00
Total	99.46	99.42	99.64	99.71	99.76
Chemical Formulae Calculated on the Basis of 16 O					
Si	3.976	3.969	3.984	3.992	3.998
Zr	4.024	3.969	3.955	3.923	3.891
Th	0.000	0.000	0.000	0.055	0.040
Hf	0.000	0.000	0.061	0.000	0.042
U	0.000	0.062	0.000	0.030	0.028

bdl = below detection limit.

**Table 8.** Representative microanalyses (wt %) and calculated formulae of titanite from the black sands at Kavala.

	KVL2 1.6	KVL2 7.1	KVL5 2 9.1	KVL5 10.1	KVL5 1.5	KVL5 4.6
SiO <sub>2</sub>	30.83	30.55	31.22	30.39	30.79	30.84
TiO <sub>2</sub>	38.09	39.17	36.98	37.47	38.10	38.64
Al <sub>2</sub> O <sub>3</sub>	1.59	0.92	2.40	1.84	1.78	1.42
FeO	1.61	1.63	bdl	4.50	1.66	1.47
MnO	bdl	0.52	0.27	bdl	bdl	bdl
MgO	bdl	bdl	bdl	bdl	bdl	0.29
CaO	26.28	25.87	28.82	24.14	26.42	26.62
V <sub>2</sub> O <sub>5</sub>	0.62	bdl	bdl	bdl	0.57	bdl
Nb <sub>2</sub> O <sub>5</sub>	0.66	0.87	bdl	1.03	bdl	0.55
Total	99.68	99.52	99.69	99.37	99.88	99.82
Chemical Formulae Calculated on the Basis of 4 O						
Si	4.000	4.000	4.000	4.000	4.000	4.000
Ti	3.716	3.856	3.563	3.708	3.722	3.768
Al	0.243	0.142	0.362	0.285	0.273	0.216
Y	3.959	3.998	3.925	3.994	3.995	3.985
Fe	0.174	0.178	0.000	0.496	0.180	0.159
Mn	0.000	0.058	0.030	0.000	0.000	0.000
Mg	0.000	0.000	0.000	0.000	0.000	0.056
Ca	3.654	3.629	3.956	3.404	3.677	3.698
V	0.065	0.000	0.000	0.108	0.060	0.000
Nb	0.106	0.140	0.000	0.000	0.090	0.088
X	3.999	4.004	3.986	4.008	4.007	4.001

bdl= below detection limit.

## 5. Discussion

Numerous mineralogical and geochemical studies have been carried out at the coastal areas of the Kavala district so far, demonstrating elevated concentrations in rare earths, uranium and thorium [12–21]. For more than 30 years, the Institute of Geological and Mineral Exploration (IGME, today EAGME) in collaboration with the Hellenic Centre for Marine Research (ELKETHE), have been conducting an extended exploration project on the sediments of the Northern Aegean for REE, focusing on allanite, monazite and

zirconium [13,14]. The sediments contain up to 0.8 g/t LREE, mainly lanthanum (La), cerium (Ce) and neodymium (Nd) [14]. According to Stouraiti et al. [21], the maximum extraction proportion of rare earths with magnetic separation from the coastal black sands at Kavala district can reach up to 92% in La, up to 91% Ce and up to 87% in Nd.

Previous studies have shown elevated radioactivity reaching 4488 Bq/kg, which is the highest ever measured in sediments of Greece [17,20]. The sediments offer the opportunity for detailed characterization of allanite-(Ce) and REE-rich epidote from placer deposits regarding the zoning behavior, and the partition coefficients that describe the alteration and the mechanism of chemical zoning.

The present study of the magnetic fraction of the black sands at Kariani, Pírgos, Mirtofito, Eleochori, Agia Marina and Nea Peramos of the Kavala district showed that the mineralogical composition consists of amphibole, epidote, hematite, goethite, mica, allanite-(Ce), garnet, titanite, zircon, monazite-(Ce), monazite-(La), ilmenite, rutile, magnetite, chlorite and thorite. The major REE-bearing minerals are allanite-(Ce), 2–5 wt % of the total magnetic fraction, and epidote. Monazite and thorite contribute to a lesser extent in the REE content. Similar results were previously presented by [19–21]. LA-ICP-MS analysis conducted by [18–20] demonstrated that titanite and zircon also contain traces of REE.

The quantity of the REE-bearing minerals shows strong fluctuations depending on the proximity of the beaches to the Kavala pluton (Figure 1), which is considered the main source for allanite-(Ce), REE-rich epidote, epidote, monazite-(Ce), monazite-(La) and thorite. The KVL1 sample from Kariani, which was collected at a rather long distance from the pluton, has the lowest allanite-(Ce) and epidote concentrations. The main component is garnet, possibly implying a source from the metamorphic rocks, especially gneiss, of the broader area. The maximum quantity of allanite-(Ce) was found in sample KVL4 at Eleochori (Table 3).

Allanite is the compositionally most diverse part of the epidote group. In the A2 sites,  $\text{Ca}^{2+}$  is replaced by trivalent REE, Th and U. This incorporation of  $\text{REE}^{3+}$  is charge-balanced by divalent cation substitutions for trivalent cations in the M sites, according to the exchange  $\text{A}2^{2+} + \text{M}3^{3+} \leftrightarrow \text{A}2^{3+} + \text{M}3^{2+}$  [38,45]. More precisely,  $\text{Al}^{3+}$  and  $\text{Fe}^{3+}$  are substituted by  $\text{Fe}^{2+}$ ,  $\text{Mg}^{2+}$  and  $\text{Mn}^{2+}$  in the unit cell of allanites of Kavala. These cation exchanges are plotted in Figure 8a, and are characterized by a negative trend line, indicating that the exchange mechanism is  $(\text{Ca} + (\text{Fe}^{3+}, \text{Al}))_{-1}(\text{LREE}, \text{Y}, \text{Th}, \text{U} + (\text{Fe}^{2+}, \text{Mg}, \text{Mn}))_{+1}$  [37]. The exchange vector specifies the 1:1 substitution mechanism. The strong negative correlation of the cations in the alkali site A2 proves the considerable substitution between  $\text{LREE} + \text{Y} + \text{Th} + \text{U}$  and Ca (Figure 8b).

A positive correlation is evident between  $\text{Fe}^{2+} + \text{Mg} + \text{Mn}$  and  $\text{LREE} + \text{Y} + \text{Th} + \text{U}$  (Figure 8c). The cation  $\text{Fe}^{2+}$  in the M3 site expands the allanite structure to accommodate REE in the A2 site. Magnesium and Mn in the M3 site compensate for this charge imbalance. Figure 8d indicates less participation of the substitution mechanism of  $\text{Al} + \text{Fe}^{3+}$  vs.  $\text{LREE} + \text{Y} + \text{Th} + \text{U}$ .

The epidote-group minerals found in the Kavala black sands are suggested to originate from the adjacent Miocene Kavala pluton. In many grains, allanite-(Ce) occur as cores that progressively lapse into REE-rich epidote and finally to epidote in the rims. This zoning structure possibly reflects the melt depletion of LREE and fractionation in allanite, from the core to the rim, a process that is common in magmatic rocks, as has been previously suggested by [38]. In addition, some allanite-(Ce) grains reveal patchy internal textures, displaying darker and lighter gray domains with irregular limits in the SEM-BSE images. The low BSE intensity is ascribed to REE leaching in allanite-(Ce), and has been described by [47]. This chemical variation is possibly generated by hydrothermal fluids that penetrated allanite along grain fractures.

The elevated Th content indicates that the allanite is metamict, and resulted in the LREE leaching and the enrichment of Th, and Y in some crystals. The negative cation correlation plots of epidote mineral group (Figure 8a) suggest that the alteration is related to the chemical exchange mechanism between the primary allanite-(Ce) and the

hydrothermal fluids, and is described by the reaction:  $\text{LREE}^{3+} + \text{Fe}^{2+} \leftrightarrow \text{Ca}^{2+} + \text{Al}^{3+}$  [47,48]. This is documented by the mode of occurrence of thorite and monazite–cheralite, which are found locally along the cracks of the allanite-(Ce) grains. These mineral phases were formed after allanite-(Ce) formation, due to fluid circulation that removed the REE and re-precipitated them in these cracks [47–49].

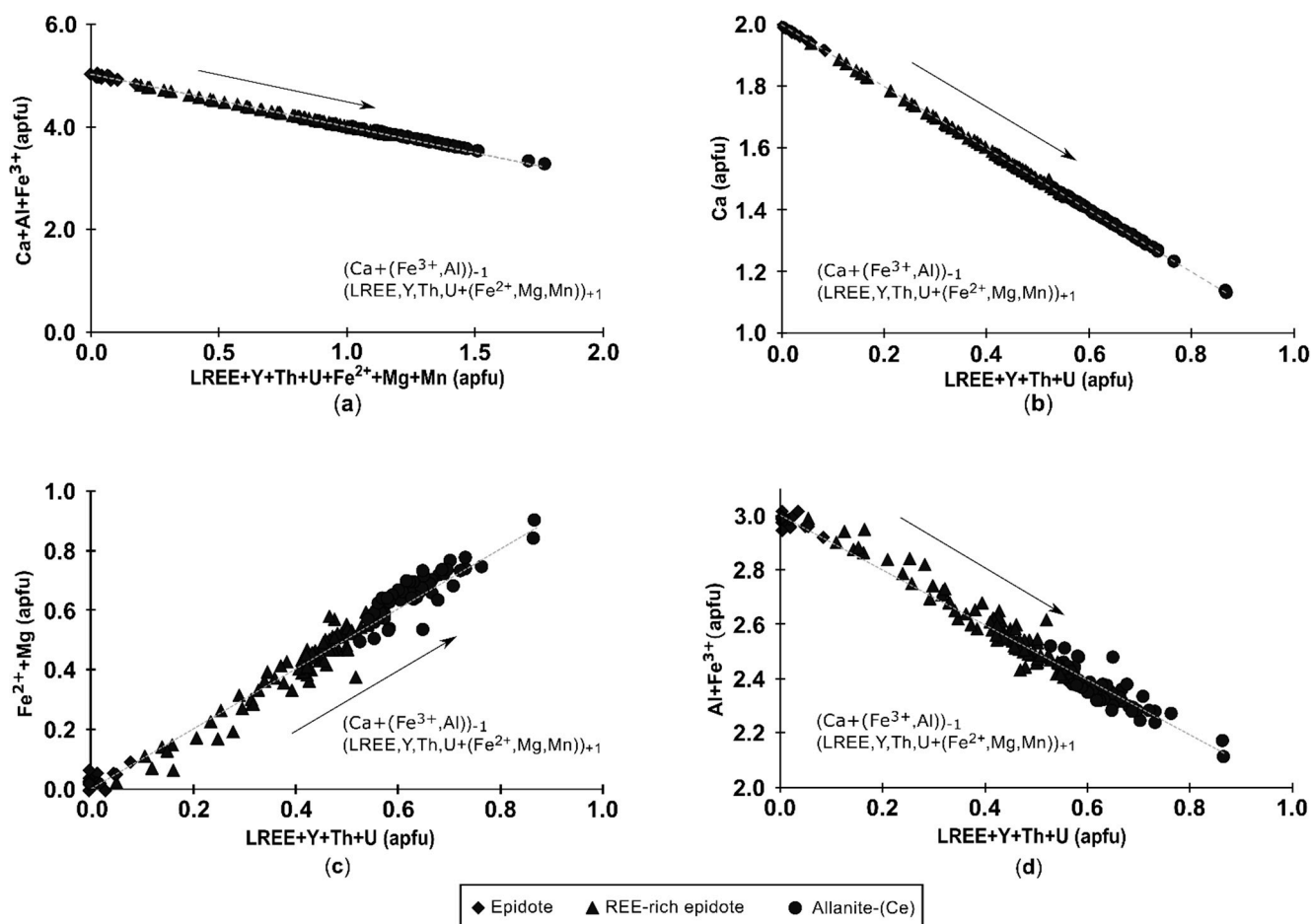


**Figure 8.** Plots showing possible cationic substitutions in epidote mineral group structure indicated for the Kavala black sands: (a)  $\text{Ca}+\text{Al}+\text{Fe}^{3+}$  vs.  $\text{LREE}+\text{Y}+\text{Th}+\text{U}+\text{Fe}^{2+}+\text{Mg}+\text{Mn}$ ; (b)  $\text{Ca}$  vs.  $\text{LREE}+\text{Y}+\text{Th}+\text{U}$ ; (c)  $\text{Fe}^{2+}+\text{Mg}+\text{Mn}$  vs.  $\text{LREE}+\text{Y}+\text{Th}+\text{U}$ ; (d)  $\text{Al}+\text{Fe}^{3+}$  vs.  $\text{LREE}+\text{Y}+\text{Th}+\text{U}$ .

The plots of the three most abundant rare earths (Ce, La, Nd) versus  $\Sigma\text{REE}$  in the epidote-group minerals at Kavala show different decreasing trends, depending on the abundance and the atomic number of these elements. There is a strong positive correlation of the  $\Sigma\text{REE}$  with Ce and La (Figure 9a,b) demonstrating that these two elements dominate among the REE in the epidote-group minerals from the Kavala black sands. Neodymium shows a slight positive correlation with  $\Sigma\text{REE}$  (Figure 9c), suggesting a minor incorporation.

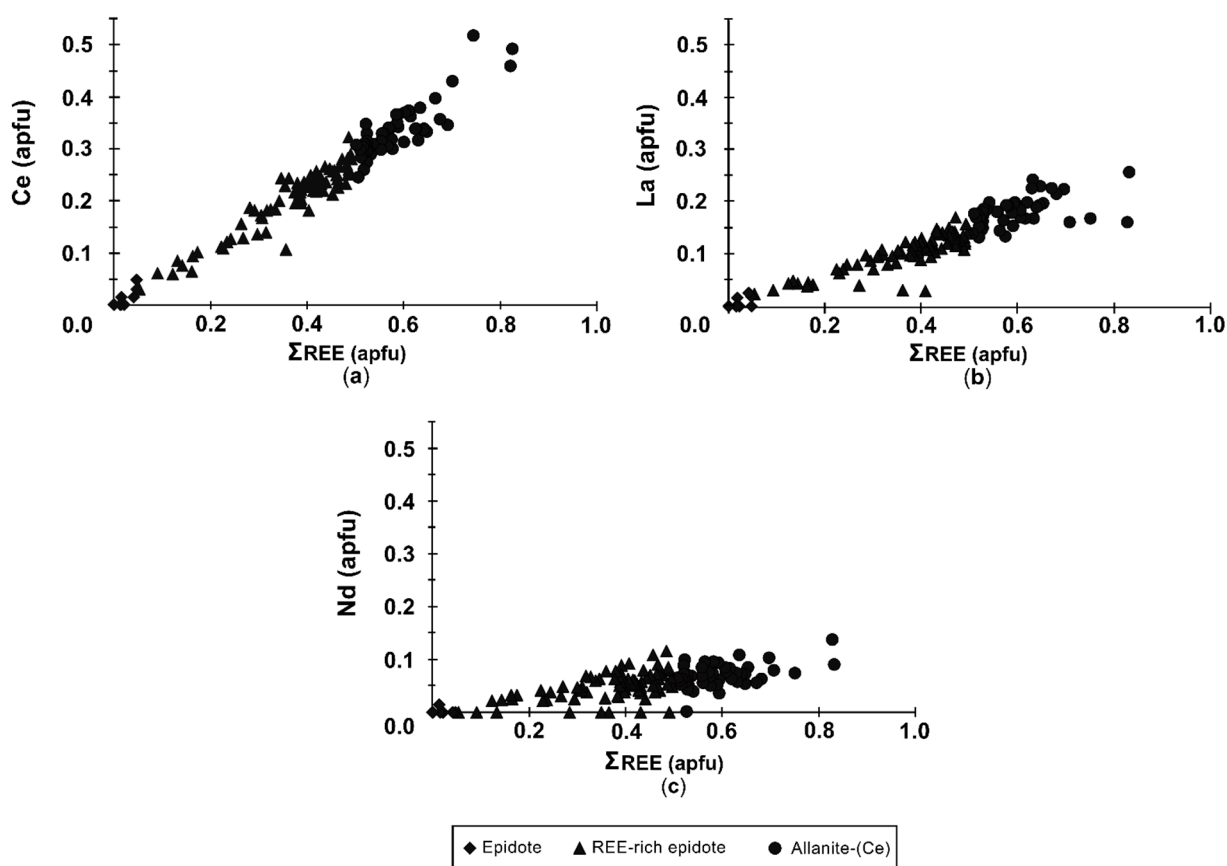


**Figure 9.** Plots showing the correlations between (a) Ce vs.  $\Sigma$ REE; (b) La vs.  $\Sigma$ REE and (c) Nd vs.  $\Sigma$ REE in the epidote-group minerals from the Kavala black sands.

## 6. Conclusions

The mineralogical study of the magnetic fraction from the coastal black sands at Kavala district, Northern Greece, revealed the presence of allanite (2–5% wt) as the major host mineral for LREE (La, Ce, Nd), Th and U. Low REE concentrations were also observed in the REE-rich epidote, in monazite, and in thorite. Cerium dominates among the other rare earths, and thus the allanites of the black sand are identified as allanite-(Ce). The high Th content and the elevated  $Fe_{ox}$  (>0.5) are common in the metamictic allanites. The epidote-group minerals show a clear substitution between  $Ca + (Fe^{3+}, Al)$  and LREE, Y, Th, U +  $(Fe^{2+}, Mg, Mn)$ , which is correlated with the zoning patterns among allanite-(Ce), REE-rich epidote and epidote in single grains.

**Author Contributions:** Conceptualization, V.M. and E.P.; methodology, E.P., L.P. and N.K.; software, E.P.; validation, E.P., V.M., L.P., N.K. and P.V.; formal analysis, E.P.; investigation, E.P., L.P. and N.K.; data curation, E.P., V.M., L.P., N.K. and P.V.; writing—original draft preparation, E.P.; writing—review and editing, V.M., L.P., N.K. and P.V.; supervision, V.M.; funding acquisition, E.P. All authors have read and agreed to the published version of the manuscript.

**Funding:** E.P. received a scholarship founded by HELLENIC PETROLEUM S.A. through the Special Account for Research Grants (S.A.R.G.) A.U.Th. in the context of the project No 98665 “Graduate Student Scholarships with the support of ELPE- 2019” (MIS-547370).

**Data Availability Statement:** Not applicable.

**Acknowledgments:** The present study was carried out within the framework of the master thesis of the first author, Eftychia Peristeridou, who has been financially supported by HELLENIC PETROLEUM S.A. (HELPE). Special thanks should be addressed to Christos Stergiou for his assistance during sampling.

**Conflicts of Interest:** The authors declare no conflict of interest. The funders had no role in the design of the study; in the collection, analyses or interpretation of data; in the writing of the manuscript, or in the decision to publish the results.

## References

1. Watari, T.; McLellan, B. C.; Giurco, D.; Dominish, E.; Yamasue, E.; Nansai, K. Total material requirement for the global energy transition to 2050: A focus on transport and electricity. *Resources, Conservation and Recycling* **2019**, *148*, 91–103. <https://doi.org/10.1016/j.resconrec.2019.05.015>.
2. European Commission. Critical Raw Materials Resilience: Charting a Path towards Greater Security and Sustainability; European Commission: Brussels, Belgium, 2020; p. 4.
3. Emsley, J. *Nature's building blocks: an AZ guide to the elements*, 2nd ed. Oxford University Press, 2011.
4. Van Gosen, B. S.; Verplanck, P. L.; Seal II, R. R.; Long, K. R.; Gambogi, J. Rare-Earth Elements, chap. 0 in *Critical mineral resources of the United States: economic and environmental geology and prospects for future supply*, No. 1802-O; Schulz, K. J.; DeYoung, J. H.; Seal, R. R.; Bradley, D. C., Eds.; U.S. Geological Survey Professional Paper 1802: Virginia, U.S.A., 2018; pp. 1-31. <https://doi.org/10.3133/pp1802O>.
5. Dushyantha, N.; Batapola, N.; Ilankoon, I.M.S.K.; Rohitha, S.; Premasiri, R.; Abeysinghe, B.; Ratnayake, N.; Dissanayake, K. The story of rare earth elements (REEs): Occurrences, global distribution, genesis, geology, mineralogy and global production. *Ore Geology Reviews* **2020**, *122*, 103521. <https://doi.org/10.1016/j.oregeorev.2020.103521>
6. Goodenough, K. M.; Schilling, J.; Jonsson, E.; Kalvig, P.; Charles, N.; Tuduri, J.; Deady, E. A.; Sadeghi, M.; Schiellerup, H.; Müller, A.; Bertrand, G.; Arvanitidis, N.; Eliopoulos, D. G.; Shaw, R. A.; Thrane, K.; Keulen, N. Europe's Rare Earth Element Resource Potential: An Overview of REE Metallogenic Provinces and Their Geodynamic Setting. *Ore Geology Reviews* **2016**, *72*, 838–856. <https://doi.org/10.1016/j.oregeorev.2015.09.019>.
7. Barakos, G.; Gutzmer, J.; Mischo, H. Strategic evaluations and mining process optimization towards a strong global REE supply chain. *Journal of Sustainable Mining* **2016**, *15*, 26–35. <https://doi.org/10.46873/2300-3960.1194>.
8. Verplanck, P. L.; Hitzman, M. W. Rare Earth and Critical Elements in Ore Deposits; *Reviews in Economic Geology* **2016**, *18*, 1–3. <https://doi.org/10.5382/rev.18>.
9. Long, K. R.; van Gosen, B. S.; Foley, N. K.; Cordier, D. The Principal Rare Earth Elements Deposits of the United States: A Summary of Domestic Deposits and a Global Perspective. In *Non-Renewable Resource Issues: Geoscientific and Societal Challenges*; Sinding-Larsen, R.; Wellmer, F. W., Eds.; Springer: 2012; pp. 131-156. [https://doi.org/10.1007/978-90-481-8679-2\\_7](https://doi.org/10.1007/978-90-481-8679-2_7).
10. Castor, S. B.; Hedrick, J. B. Rare earth elements. *Industrial Minerals & Rocks* **2006**, pp. 769-792. [10.1002/9781119951438.eibd0664](https://doi.org/10.1002/9781119951438.eibd0664)
11. Jordens, A.; Cheng, Y. P.; Waters, K. E. A Review of the Beneficiation of Rare Earth Element Bearing Minerals. *Minerals Engineering* **2013**, *41*, 97–114. <https://doi.org/10.1016/j.mineng.2012.10.017>.
12. Papadakis, A. The black sands of Loutra Eleftheron near Kavala, Greece. *Sci. Ann. Fac. Phys. Math. Univ. of Thessaloniki* **1975**, *15*, 331–390.
13. Perissoratis, C.; Moorby, S. A.; Angelopoulos, I.; Cronan, D. S.; Papavasiliou, C.; Konispoliatis, N.; Sakellariadou, F.; Mitropoulos, D. Mineral Concentrations in the Recent Sediments Off Eastern Macedonia, Northern Greece: Geological and Geochemical Considerations. In *Mineral Deposits within the European Community*; 1988. [https://doi.org/10.1007/978-3-642-51858-4\\_29](https://doi.org/10.1007/978-3-642-51858-4_29).
14. Pergamalis, F.; Karageorgiou, D.E.; Koukoulis, A.; Katsikis, I. Mineralogical and chemical composition of sand ore deposits in the seashore zone N. Peramos-L. Eleftheron (N. Greece). *Bulletin of the Geological Society of Greece* **2001**, *34*, 845–850. <https://doi.org/10.12681/bgsg.17091>
15. Pergamalis, F.; Karageorgiou, D.E.; Koukoulis, A. The location of Ti, REE, Th, U, Au deposits in the seafront zones of Nea Peramos-Loutra Eleftheron area, Kavala (N. Greece) using radiation. *Bulletin of the Geological Society of Greece* **2001**, *34*, 1023–1029. <https://doi.org/10.12681/bgsg.17707>
16. Aggelatou, V.; Papamanoli, S.; Stouraiti, C.; Papavasileiou, K. REE distributions in the black sands of Kavala coastal zone, northern Greece: mineralogical and geochemical characterization of beneficiation products. Proceedings of the 1<sup>st</sup> International Electronic Conference on Mineral Science, 2018, vol 1, 1. <https://doi.org/10.3390/IECMS2018-05455>.
17. Papadopoulos, A.; Koroneos, A.; Christofides, G.; Stoulos, S. Natural Radioactivity Distribution and Gamma Radiation Exposure of Beach Sands Close to Kavala Pluton, Greece. *Open Geosciences* **2015**, *7*, 407–422. <https://doi.org/10.1515/geo-2015-0043>.
18. Papadopoulos, A.; Koroneos, A.; Christofides, G.; Papadopoulou, L. Geochemistry of Beach Sands from Kavala, Northern Greece. *Italian Journal of Geosciences* **2016**, *135*, 526–539. <https://doi.org/10.3301/IJG.2016.01>.
19. Papadopoulos, A.; Tzifas, I. T.; Tsikos, H. The Potential for REE and Associated Critical Metals in Coastal Sand (Placer) Deposits of Greece: A Review. *Minerals* **2019**, *9*, 469 <https://doi.org/10.3390/min9080469>.
20. Tzifas, I. T.; Papadopoulos, A.; Misaelides, P.; Godelitsas, A.; Göttlicher, J.; Tsikos, H.; Gamaletsos, P. N.; Luvizotto, G.; Karydas, A. G.; Petrelli, M.; Noli, F.; Kantarelou, V.; Kontofakas, A.; Hatzidimitriou, A. New Insights into Mineralogy and Geochemistry of Allanite-Bearing Mediterranean Coastal Sands from Northern Greece. *Chemie der Erde* **2019**, *79*, 247–267 <https://doi.org/10.1016/j.chemer.2019.05.002>.

21. Stouraiti, C.; Angelatou, V.; Petushok, S.; Soukis, K.; Eliopoulos, D. Effect of Mineralogy on the Beneficiation of REE from Heavy Mineral Sands: The Case of Nea Peramos, Kavala, Northern Greece. *Minerals* **2020**, *10*, 387 <https://doi.org/10.3390/min10050387>.
22. Kromberg, P.; Schenk, P. F. Nikisiani- Loutra Elevtheron Sheets. *Geological Map of Greece, Scale 1:50.000*; Institute of Geology and Mineral Exploration (IGME): Athens, Greece, 1974.
23. Xidas, S. Rodholivos Sheet. *Geological Map of Greece, Scale 1:50.000*; Institute of Geology and Mineral Exploration (IGME): Athens, Greece, 1984.
24. Kromberg, P. Kavala Sheet. *Geological Map of Greece, Scale 1:50.000*; Institute of Geology and Mineral Exploration (IGME): Athens, Greece, 1973.
25. Brun, J. P.; Sokoutis, D. Kinematics of the Southern Rhodope Core Complex (North Greece). *International Journal of Earth Sciences* **2007**, *96*, 1079–1099. <https://doi.org/10.1007/s00531-007-0174-2>.
26. Kounov, A.; Wüthrich, E.; Seward, D.; Burg, J. P.; Stockli, D. Low-Temperature Constraints on the Cenozoic Thermal Evolution of the Southern Rhodope Core Complex (Northern Greece). *International Journal of Earth Sciences* **2015**, *104*, 1337–1352 <https://doi.org/10.1007/s00531-015-1158-2>.
27. Dinter, D. A.; Macfarlane, A.; Hames, W.; Isachsen, C.; Bowring, S.; Royden, L. U-Pb and  $^{40}\text{Ar}/^{39}\text{Ar}$  Geochronology of the Symvolon Granodiorite: Implications for the Thermal and Structural Evolution of the Rhodope Metamorphic Core Complex, North-eastern Greece. *Tectonics* **1995**, *14*, 886–908. <https://doi.org/10.1029/95TC00926>.
28. Dinter, D. A. Late Cenozoic Extension of the Alpine Collisional Orogen, Northeastern Greece: Origin of the North Aegean Basin. *Bulletin of the Geological Society of America* **1998**, *110*, 1208–1230. [https://doi.org/10.1130/0016-7606\(1998\)110<1208:LCE-OTA>2.3.CO;2](https://doi.org/10.1130/0016-7606(1998)110<1208:LCE-OTA>2.3.CO;2).
29. Neiva, A. M. R.; Christofides, G.; Eleftheriadis, G.; Soldatos, T. Geochemistry of Granitic Rocks and Their Minerals from the Kavala Pluton, Northern Greece. *Chemie der Erde* **1996**, *56*, 117–142.
30. Christofides, G.; Neiva, A. M. R.; Soldatos, T.; Eleftheriadis, G. (1995). Petrology of the Kavala plutonite (Eastern Macedonia, Greece). In *Proceedings of the XV Congress CBGA 1995*, pp. 489–494.
31. Xydous, S.; Magganas, A.; Pomonis, P.; Kokkinakis, A. Tourmalinite veins and breccias from the Symvolon-Kavala pluton, northern Greece: petrogenetic preliminary results. *Bulletin of the Geological Society of Greece* **2016**, *50*, 2079–2087. <https://doi.org/10.12681/bgsg.14259>
32. Dinter, D. A.; Royden, L. Late Cenozoic Extension in Northeastern Greece: Strymon Valley Detachment System and Rhodope Metamorphic Core Complex. *Geology* **1993**, *21*, 45–48. [https://doi.org/10.1130/0091-7613\(1993\)021<0045:LCEING>2.3.CO;2](https://doi.org/10.1130/0091-7613(1993)021<0045:LCEING>2.3.CO;2).
33. Kokkinakis, A. Geologie und Petrographie des Kavala-Gebietes und des Symvolongebirges in Griechisch-Ostmakedonien. *Zeitschrift der deutschen geologischen Gesellschaft* **1980**, *131*, 903–925.
34. Kyriakopoulos, K.; Pezzino, A.; Del Moro, A. Rb-Sr geochronological, petrological and structural study of the Kavala plutonic complex (N. Greece). *Bulletin of the Geological Society of Greece* **1989**, *23*, 545–560.
35. Doebelin, N.; Kleeberg, R. Profex: a graphical user interface for the Rietveld refinement program BGMN. *Journal of applied crystallography*, **2015**, *48*, 1573–1580.
36. Dollase, W. a. Refinement of the Crystal Structures of Epidote, Allanite and Hancockite. *The American Mineralogist* **1971**, *56*.
37. Deer, W. A.; Howie, R. A.; Zussman, J. Rock-forming minerals. *Disilicates and ring silicates*, 2<sup>nd</sup> ed.; Longman: Harlow, United Kingdom, 1997; 629 p.
38. Gieré, R.; Sorensen, S. S. Allanite and Other: REE-Rich Epidote-Group Minerals. *Reviews in Mineralogy and Geochemistry* **2004**, *56*, 431–493. <https://doi.org/10.2138/gsrng.56.1.431>.
39. Armbruster, T.; Bonazzi, P.; Akasaka, M.; Bermanec, V.; Chopin, C.; Gieré, R.; Heuss-Assbichler, S.; Liebscher, A.; Menchetti, S.; Pan, Y.; Pasero, M. Recommended Nomenclature of Epidote-Group Minerals. *European Journal of Mineralogy* **2006**, *18*, 551–567. <https://doi.org/10.1127/0935-1221/2006/0018-0551>.
40. Thomson, T. Experiments on allanite, a new mineral from Greenland. *Trans. Royal Soc. Edinburg*, **1810**, *8*, 371–386.
41. Franz, G.; Liebscher, A. Physical and Chemical Properties of the Epidote Minerals-An Introduction-. *Reviews in Mineralogy and Geochemistry* **2004**, *56*, 1–82. <https://doi.org/10.2138/gsrng.56.1.1>.
42. Graser, G.; Markl, G. Ca-Rich Ilvaite-Epidote-Hydrogarnet Endoskarns: A Record of Late-Magmatic Fluid Influx into the Per-sodic Ilímaussaq Complex, South Greenland. *Journal of Petrology* **2008**, *49*, 239–265. <https://doi.org/10.1093/petrology/egm079>.
43. Ercit, T. S. The Mess That Is “Allanite.” *Canadian Mineralogist* **2002**, *40*, 1411–1419. <https://doi.org/10.2113/gscanmin.40.5.1411>.
44. Kartashov, P. M.; Ferraris, G.; Ivaldi, G.; Sokolova, E.; McCammon, C. A. Ferriallanite-(Ce),  $\text{CaCeFe}^{3+}\text{AlFe}^{2+}(\text{SiO}_4(\text{Si}_2\text{O}_7)\text{O}(\text{OH}))$ , a new member of the Epidote Group: Description, X-Ray and Mössbauer Study. *Canadian Mineralogist* **2003**, *41*, 829–830.
45. Petrik, I.; Broska, I.; Lipka, J.; Siman, P. Granitoid Allanite-(Ce): Substitution Relations, Redox Conditions and REE Distributions (on an Example of I-Type Granitoids, Western Carpathians, Slovakia). *Geologica Carpathica* **1995**, *46*, 79–94.
46. Mills, S. J.; Hatert, F.; Nickel, E. H.; Ferraris, G. The Standardisation of Mineral Group Hierarchies: Application to Recent Nomenclature Proposals. *European Journal of Mineralogy* **2009**, *21*, 1073–1080. <https://doi.org/10.1127/0935-1221/2009/0021-1994>.

47. Poitrasson, F. In Situ Investigations of Allanite Hydrothermal Alteration: Examples from Calc-Alkaline and Anorogenic Granites of Corsica (Southeast France). *Contributions to Mineralogy and Petrology* 2002, 142, 485–500. <https://doi.org/10.1007/s004100100303>.
48. Chen, W. T.; Zhou, M. F. Ages and Compositions of Primary and Secondary Allanite from the Lala Fe-Cu Deposit, SW China: Implications for Multiple Episodes of Hydrothermal Events. *Contributions to Mineralogy and Petrology* 2014, 168. <https://doi.org/10.1007/s00410-014-1043-1>.
49. Sawka, W. N.; Chappell, B. W.; Norrish, K. Light-Rare-Earth-Element Zoning in Sphene and Allanite during Granitoid Fractionation. *Geology* 1984, 12, 131–134. [https://doi.org/10.1130/0091-7613\(1984\)12<131:LZISAA>2.0.CO;2](https://doi.org/10.1130/0091-7613(1984)12<131:LZISAA>2.0.CO;2).